



Università degli Studi di Ferrara

DOTTORATO DI RICERCA IN
"FISICA"

CICLO XXIX

COORDINATORE Prof. Vincenzo Guidi

Radiographic imaging of chemical elements for Cultural Heritage

Settore Scientifico Disciplinare FIS/07

Dottorando

Dott. Anna Impallaria

Anna Impallaria

Tutore

Prof. Ferruccio Petrucci

F. Petrucci

Anni 2014-2016

Contents

Introduction	3
1 Background	5
1.1 Elemental maps in Archaeometry	6
1.2 K-edge differential radiography	10
1.2.1 Synchrotron	13
1.2.2 Bragg diffraction	14
1.2.3 Balanced filters	14
2 Methods and Materials	17
2.1 The goniometric setup	17
2.2 The balanced filters	27
2.3 The radiographic scanner	31
3 K-edge applications	39
3.1 Cadmium	41
3.1.1 KES technique	42
3.1.2 Lehmann Algorithm	50
3.1.3 Further tests	56
3.1.4 Conclusion	61
3.2 Copper and Cobalt	62
3.2.1 KES technique	63
3.3 Conclusion	72
Conclusion	73
A From X-radiography to Art History	75
Bibliography	93

Introduction

In the field of Cultural Heritage, from many years, the use of scientific techniques to study the materials composing works of art is a stabilized routine before restorations, to obtain information concerning the Art History or the artistic technique.

Mapping the elemental distribution of elements, is especially efficient, not only for the identification of the materials (pigments), but also for pointing out their use by the artist.

The K-edge differential radiography allows to obtain the distribution of a target element through all the thickness of the painting analysed. It takes advantage on the sharp rise of X-ray absorption coefficient, the K-edge discontinuity. Acquiring two images with monochromatic X-ray beams with energy below and over the K-edge of the target element, the main difference between them is due to the presence of the element itself.

The Archaeometry group of the Dept. of Physics and Earth Science of the University of Ferrara, in collaboration with INFN, has examined two ways to obtain the K-edge radiography using common X-ray tubes. The first considers the monochromatization of the X-ray beam via Bragg diffraction (goniometric setup), the second exploits the differences among three images acquired filtering the X-ray beam with elemental filters.

In the first chapter, after a brief comparison of some techniques used for elemental maps, the K-edge radiography and the ways to carry it out are explained.

In the second chapter, the instruments developed during my PhD period are illustrated, stressing the last upgrades about their portability.

In the third chapter, some applications of the balanced filters K-edge radiography are shown for cadmium, copper and cobalt mock-ups and the results are discussed.

Chapter 1

Background

In the field of cultural heritage, many techniques are used detecting the elemental composition of materials. Some of them are non-invasive (or micro-invasive) and non-destructive, which are the main requests when working on Cultural Heritage. Thus, the identification of materials is possible thanks to the interpretation of spectra which come from various spot analyses, such as Ion Beam Analysis (IBA), X-ray Fluorescence (XRF), Raman spectroscopy, etc.

Keeping in mind that materials employed in art are extremely heterogeneous, even at the micrometric scale, the choice of the points to be analysed could become tricky because they could be not representative of the real composition. If so, the results give misleading or ambiguous information, when a comprehensive knowledge of the materials composing the work of art is requested.

Hence, it is necessary to collect a large number of samples to characterize precisely the artistic material, even if the pigment used are limited and typical of a specific historic period. An example is the Trichiana Altarpiece (Figure 1.1): an Altarpiece of the Venetian Renaissance with dimensions of 238 x 176 cm, painted by Giovanni Da Mel for the church of Trichiana (Prealps of Belluno). To identify all the pigments used by the artist and their mixture, more than one hundred points have been acquired *in situ* with a XRF spectrometer and cross-correlation has been investigated with a similar collection of spectrophotometric measurements. [1]

As you can see from the Figure 1.1b, many points analysed are really close to each other, because it is important to understand which are the causes of small differences in colour appearance. That is, if they are due to the use of different pigments or if they have been slightly corrected by the artist himself. Furthermore, the presence of restoration material in some areas has incremented the number of collected points, in order to avoid misleading data. In these situations the use of distribution maps of elements are helpful and clarifying and their interpretation easier.



Figure 1.1: a)Trichiana Altarpiece, b) maps of all the points analysed

For this reason, in the last decade, many efforts have been done in order to reconstruct the space distribution of elements over an area. The compositional maps give more significant data than single spot analysis, therefore the problem of choosing representative points is overcome.

1.1 Elemental maps in Archaeometry

Conservators, restorers, curators and art historians turn to the scientific techniques and, in particular, to element maps, because knowing the materials and their spatial distribution can give information about:

- the artistic technique, answering to questions related to the Art History;
- the presence of restorations and retouches, to reconstruct the History of the artwork analysed;
- the authenticity and the dating, when a proof about them is requested.

The questions can be of various nature and for each of them, the best technique to use and in which conditions, can be identified.

Speaking about elemental maps, it is important to take into account some characteristics of the employed techniques. First of all, we have to consider which and how many elements can be revealed. For example, working with XRF spectrometer in air, it is difficult to highlight the presence of elements with $Z < 14$ (Silicon), so all the organic components are excluded by the analysis.

Then, we have to consider the spatial resolution of the maps: in some cases it is enough a low definition. In others, more detailed images are requested. Resolution is often correlated with the acquiring time: using the same instrument, increasing the resolution means increasing the time too. Also the dimension of the analysed area is something to take into account, especially when big areas have to be covered.

Finally, the portability of the instruments is an important task for Cultural Heritage, because the movement of works of art is often denied.

In the following, some examples of elemental maps achieved with different techniques will be shown. Many of them regards Italian research units, such as Florence and Catania, frequently collaborating with the Ferrara group.

Among IBA techniques, PIXE (Particle Induced X-ray Emission) is one of the most used, because the analysis is not only qualitative but also quantitative, giving the concentration of each element (with $Z > 11$ working with external beam) present in the point analysed.

In the florentine LABEC, at the University and INFN, the scanning system has been developed at the microbeam line. In typical conditions, the beam size can be in the range between $10 \mu\text{m}$ and $100 \mu\text{m}$, and the scanned area is limited to the dimensions of the exit window. In fact, the scanning is performed sweeping the beam by means of magnets on the target surface. For example, using a beam size of $100 \mu\text{m}$ and a Upilex window 3 mm in diameter, it is possible to scan an area of $2 \times 2 \text{ mm}^2$ in 2-3 minutes. For larger areas, adjacent zones have to be combined. [2]

The scanning micro-PIXE finds application in many cases. Related to Cultural Heritage, for example, it is very useful in minerological applications, such as the provenance study of the semi-precious stone *lapis lazuli* of glyptic art [3].

Recently, a new scanning system for wider area has been implemented. Thanks to two motorized linear stages, the sample moves in front of the beam, while acquiring the spectra, in order to obtain maps up to $20 \times 20 \text{ cm}^2$. In this way the acquiring time is strongly decreased. The spatial resolution depends mainly on the beam spot size (down to $25 \mu\text{m}$) and the scanning velocity. For instance, an area of $25 \times 30 \text{ cm}^2$, with 1 mm of spatial resolution, takes a measurement time of 25 min. [4]

At the parisian accelerator, at the Louvre Museum, they coupled the magnetic deflection of the beam (up to $640 \mu\text{m}$) with the X, Y movement of the sample on motorized stage. The total scan area can be up to $20 \times 20 \text{ cm}^2$, which is the same of the LABEC set-up, but with a spatial resolution that can go down to $6 \mu\text{m} \times 3 \mu\text{m}$. For comparison, the elemental maps of a $\sim 14 \times 14 \text{ mm}^2$ area with pixel size of $64 \mu\text{m}$ have been acquired in 90 min. [5] [6]

Due to the use of microbeams, both the facilities have the possibility to perform the mapping of elements with very high spatial resolution and the time is depending on the area acquired and the pixel size. Even if the advantages of IBA imaging are evident, the main problem is that they are not portable, and very often an art work is not allowed to be moved to the lab.

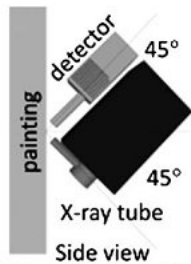
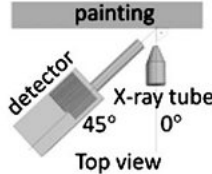
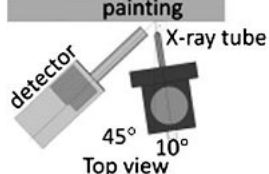
The largely used technique in Cultural Heritage to identify the materials *in situ* is XRF, another multi-elemental technique as PIXE. If an unvaried flux of Helium is used in front of the sample, XRF can reveal the presence of all the element with $Z > 11$. Again, the technique is blind to all the organic elements. Starting as spot analysis, in the last years it has been implemented to achieve elemental maps by various research groups. We will focus on two main solutions: the scanning and the full field mode.

For the first one, the examples of LABEC in Florence (Italy), the University of Antwerp (Belgium) and LANDIS in Catania systems will be presented. The scanning systems can acquire the spectra, while the system is moving or in dwell mode.

At LABEC, the XRF scanner acquires the X-ray spectra and the spatial coordinates while moving on the area to be analysed. The maximum scanned area achievable is $20 \times 20 \text{ cm}^2$ and the spatial resolution depends on the collimator used (typically 0.3 or 1 mm) and on the scanning velocity. For the case of "La Muta" by Raffaello [7], twenty-one maps (covering totally 240 cm^2) have been obtained in 6 h 42', with a spatial resolution of 1 mm and 1 mm/s scanning speed.

The Antwerp group have developed in years several scanning instruments working in dwell mode (*i.e.* acquiring spectra when the motion is stopped), each one taking advantage of the previous device. In the table (Figure1.2) some specification of the scanning XRF instruments are reported. The Instrument A can work with a polycapillary lens with a spot beam of $50 \mu\text{m}$ at the focus but it is usually equipped with a Pb collimator of $700 \mu\text{m}$. Instrument B is only equipped with the same collimator, while Instrument C use the same polycapillary lens, used most of the time in defocusing mode. In Alfeld et al. [8] the development of these instruments is described in detail.

In more recent applications, the system B has been further modified in order to cover

Instrument	A	B	C
Beam-sample/detector-sample geometry ^a			
X-Ray tube	KeveX Microfocus PXS4-613	MOXTEK 50 kV "Magnum"	XOS X-beam Powerflux
Anode	Mo	Rh	Mo
Detector electronics	Inspector CSERF (Canberra)	DXP-XMAP (XIA)	DXP-XMAP (XIA)
Travel range of motors/cm ²	10 x 10	60 x 25 (hor. x vert.)	60 x 25 (hor. x vert.)
Number of detectors	1	4	4

^a For the multi-detector Instruments B and C only the detector in the horizontal plane is shown.

Figure 1.2: Technical specifications of the scanning XRF instruments from [8]

wider areas (new motor stage 57 x 60 cm) and obtain higher efficacy, such as in the case of the stained-glass window depicting Saint George and Saint Michael, now at the City Museum of Bruges (Belgium) [9]. In this study, the area analysed was 57 x 58 cm², the collimator used was 0.8 mm lead pinhole and the step size was 850 μm . The dwell time for the acquisition of XRF spectra was of 200 ms. In these conditions the measurement of the interesting area took 25 hours.

The same instrument has been used also for the study of illuminated manuscripts [10], where the step size was lower (500 μm) and the dwell time longer (275 ms) than the previous case to have a better spatial resolution and more efficiency. The area analysed was 26.3 x 26 cm² and acquired in 22 h.

The first instrument developed by the research group of Catania-LNS (INFN) is similar to the ones of the University of Antwerp: it works in dwell time and has a strong polycapillary lens which allows to work in micro and macro mode. When working as micro-XRF, the high spatial resolution is due to the beam size of 26 μm . In macro-XRF mode, the beam size is about 470 μm and the scanning area can be up to 20 x 20 cm². The dwell time is 150 ms, and the acquisition time is about 6.7 h for a 400 x 400 pixel image [11].

All the XRF scanners, previously described, are prototypes developed in Research Centres, but there is also at least a commercial solution to obtain elemental maps by means of XRF: the M6 Jetstream[®] by Bruker¹. The X-ray source is equipped with polycapillary optics, which allows to have a spot size between 100 and 500 μm and a step size down to 10 μm . The performances are similar to the other scanners: for example, to cover an area of 17 x 9.5 cm² with a step size of 1.5 mm, the measurement time was 90 min [12].

¹<https://www.bruker.com> Bruker GmbH (Germany)

The Full Field XRF (FF-XRF) designed at LNS-Catania is based on the use of a pinhole-collimator (50 μm in this case) between the sample and the 2D detector. The detector is a Silicon CCD. The X-ray beam has to be enough broad to illuminate a large area of the sample. Furthermore, changing the position of the pinhole, the field of view and the spatial resolution change. For the LNS setup, the field of view can be between 2.5 x 2.5 mm^2 and 4 x 4 cm^2 , with a spatial resolution between 30 and 170 μm , respectively. To obtain an elemental map of 4 x 4 cm^2 and 170 μm pixel size, the time needed is 83 min, while for the 2.5 x 2.5 mm^2 with very high resolution (30 μm) the time employed is 19 h. [13]

In summary, even when the XRF systems are portable and give maps of all the elements revealed with good spatial resolution, the main disadvantage is the long time they require to achieve elemental maps, especially with high spatial resolution.

1.2 K-edge differential radiography

X-ray Radiography (RX) is one of the most used imaging technique applied to Cultural Heritage to investigate the inner part of works of art for conservation and restoration purposes. The information obtained by the transmitted X-ray beam depends on the different X-ray absorption coefficient of each element and its quantity in the sample. We can take advantage of it and achieve elemental maps through the use of radiography, as will be explained in the next paragraph. Furthermore RX technology gives images with very good spatial resolution in really short acquisition time and can be applied *in situ*. Use of scanning system may be provided for large sized paintings.

The K-edge differential radiography is a radiographic technique that, due to the photoelectric effect, exploits the K-edge discontinuity in the mass attenuation coefficient (μ/ρ) of an element in order to highlight the presence of that element. If we consider an element in a matrix of other ones, at the energy of its K-edge, only the element considered will have a great difference in the coefficient (Figure 1.3), while for other elements, the difference will be negligible : $\left(\frac{\Delta\mu}{\rho}\right)_{El} \gg \left(\frac{\Delta\mu}{\rho}\right)_{Other}$

So if we acquire two images with monochromatic X-rays bracketing the K-edge energy of the target element, the main difference between them is due to the presence of the element itself. Then, subtracting one image to the other, we can obtain the spatial distribution of that element in the analysed area.

At a fixed energy, the number of photons per unit area that passing trough a layer of a

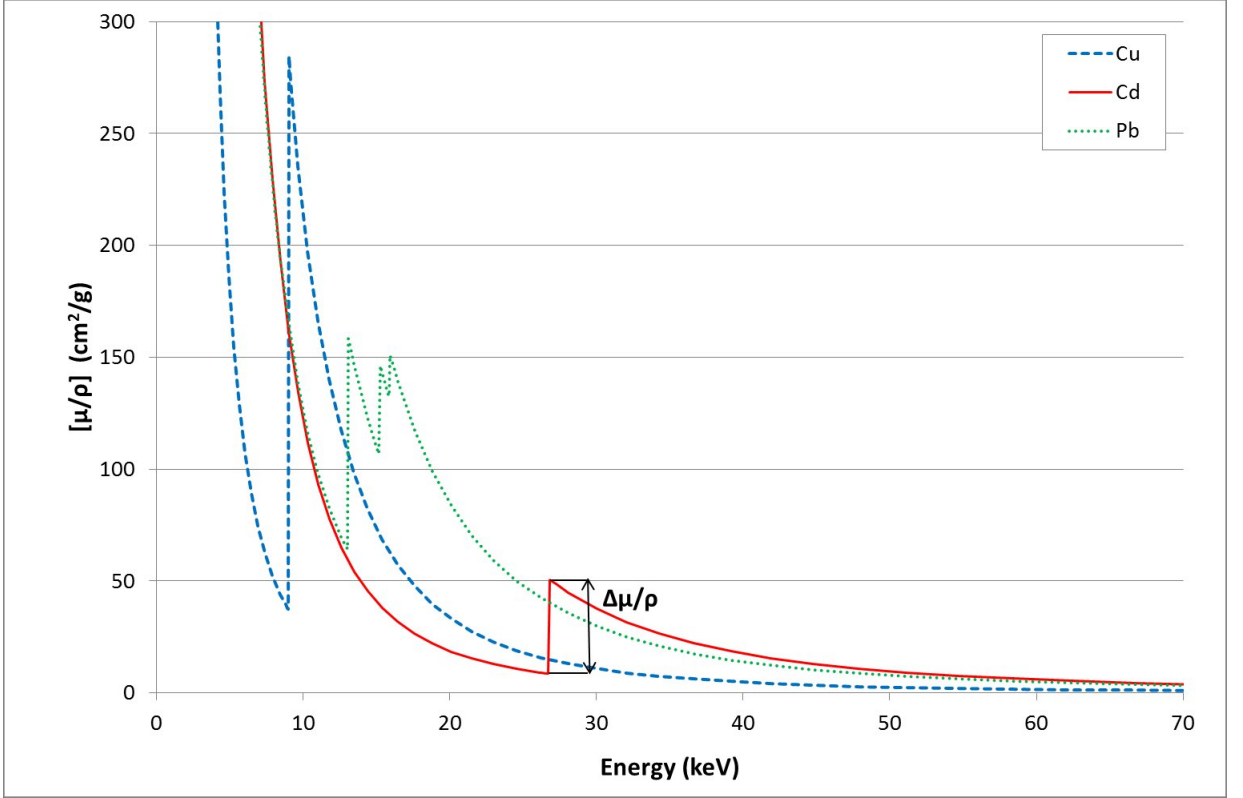


Figure 1.3: Mass attenuation coefficient of Copper, Cadmium and Lead [15]

single element is:

$$N = N_0 e^{-\mu t} \quad (1.1)$$

where N_0 is the number of incident photons, μ is the mass attenuation coefficient at that energy and t is the thickness of the element. If we acquire a *Low Energy image* ($N(E_-)$), i.e. the one obtained with monochromatic X-rays with energy under the edge of the element, and a *High Energy image* ($N(E_+)$), the one over it, we have the information below and above the edge energy of the target element. In fact, considering that:

$$\frac{N(E_-)}{N_{0E_-}} = e^{-\mu(E_-)t} \quad (1.2)$$

$$\frac{N(E_+)}{N_{0E_+}} = e^{-\mu(E_+)t} \quad (1.3)$$

where E_- and E_+ stand for low energy and high energy compared with the edge energy, their subtraction is:

$$\left(\frac{N(E_-)}{N_{0E_-}} - \frac{N(E_+)}{N_{0E_+}} \right) = e^{-\mu(E_-)t} - e^{-\mu(E_+)t} \quad (1.4)$$

depending only on μ of the element. Furthermore, $e^{-\mu(E_-)t} \approx e^{-\mu(E_+)t}$ for all other elements, while it is different from 0 for the target element. In other words, the variation

between these two images is due to the presence of the target element, while the unvaried background is due to the others. Thus, to obtain the elemental distribution of the target, it is enough to apply linear subtraction of the Low with the High image, even if the result is only qualitative. This is the so called K-Edge Subtraction (KES).

Regarding quantitative information, the Lehmann algorithm [14] has been developed to get the best discrimination between the target element and others, giving the mass density per thickness as result. The number of monoenergetic photons transmitted by the sample N per unit area, is at energies E_{\pm} :

$$N(E_{\pm}) = N_0(E_{\pm}) e^{\left\{ -\sum_i \left[\frac{\mu}{\rho}(E_{\pm}) \right]_i (\rho x)_i \right\}} \quad (1.5)$$

where:

N_0 is the number of the incident photons,

E_+ and E_- are the energies over and below the K-edge of the target element,

μ/ρ are the mass attenuation coefficient of each element i in the material,

ρx their mass density for thickness (in g/cm);

we can rewrite the sum of i in 1.5 as the sum of two components: the target element and all the others elements. In the medical field, the elements composing the matrix are low Z elements, so we can gather them in terms of an equivalent material such as water w :

$$\ln \frac{N_0}{N}(E_{\pm}) = \left[\frac{\mu}{\rho}(E_{\pm}) \right]_{El} (\rho x)_{El} + \left[\frac{\mu}{\rho}(E_{\pm}) \right]_w (\rho x)_w \quad (1.6)$$

This is a system of two equations, where the unknown quantities are ρx of both the target element and water. We can calculate them using

$$(\rho x)_{El} = \frac{\left[\frac{\mu}{\rho}(E_-) \right]_w \ln \frac{N_0}{N}(E_+) - \left[\frac{\mu}{\rho}(E_+) \right]_w \ln \frac{N_0}{N}(E_-)}{K_0} \quad (1.7)$$

$$(\rho x)_w = \frac{\left[\frac{\mu}{\rho}(E_+) \right]_{El} \ln \frac{N_0}{N}(E_-) - \left[\frac{\mu}{\rho}(E_-) \right]_{El} \ln \frac{N_0}{N}(E_+)}{K_0} \quad (1.8)$$

where K_0 is

$$K_0 = \left[\frac{\mu}{\rho}(E_-) \right]_w \left[\frac{\mu}{\rho}(E_+) \right]_{El} - \left[\frac{\mu}{\rho}(E_+) \right]_w \left[\frac{\mu}{\rho}(E_-) \right]_{El} \quad (1.9)$$

Applying 1.7 and 1.8 pixel by pixel, two images are obtained: the first is the map of the mass distribution (ρx) of the element, the second is the map of the equivalent material for all the others elements, thus the matrix.

However, we have to take into account that in paintings there are many high Z elements that cannot be considered as water, in this case, the knowledge of the "matrix" is important to evaluate the equivalent mass attenuation coefficient to be used.

Initially, the K-edge differential radiography was proposed in the medical field and was applied in angiography [16] and mammography [17]. In 2006, it was applied by Krug et al. [18] to paintings, in order to achieve the pigment distributions. The technique was performed at the synchrotron facility of Grenoble (France) acquiring a pair of RX of a test canvas at the two energies around the K-edge of the element of interest. Then, they simply subtracted the low image from the high one (KES).

The technique proved to give very useful results for paintings, in fact, working with transmitted X-rays, the target element is detected in the entire stratigraphy, even if an high Z element covers it. Furthermore, this allows to obtain information about the composition of hidden painted layers, which are of great relevance for art historians. [18]

The main task to achieve good K-edge radiographies is to employ monochromatic X-rays. There are different ways to obtain monochromatic beams and some of them are particular useful for K-edge images in terms of monochromatic beams and intensity. In the next paragraphs we will focus on the main systems applicable to paintings. They are:

- Synchrotron facilities
- Bragg diffraction, using crystals
- Balanced filters (Ross filters).

1.2.1 Synchrotron

The use of Synchrotron facilities gives the opportunity to work with very monochromatic X-rays and very intense beams. Krug et al. [18] worked at the Grenoble synchrotron with monochromatic beams in the range 20-90 keV, with dimensions of 150 x 10 mm, and acquisition time of 15-40 ms for each step. The images are therefore obtained in relative short time and with high quality and resolution.

Excluding the non portability of the instrument, the main disadvantage they occurred was the presence of significant 2^{nd} harmonic photons in the incident beam, working below 30 keV. It would decrease the K-edge image contrast and increase the noise, so they chose as target element the ones which have K-edge absorption at higher energies: cadmium, tin, antimony, barium, mercury and lead [18]. The test pattern was well mapped, but avoiding any superposition of colors and elements.

1.2.2 Bragg diffraction

Another solution can be the use of traditional X-ray tubes, which are certainly **portable**, but their beams have to be monochromatized in order to apply the K-edge differential radiography.

Monochromatization can be done via Bragg diffraction. The mono-crystal would select a narrow energy band, and the overall flux of the X-ray tube would be strongly reduced, requiring longer time of acquisition. Furthermore, the shape of the emerging beam is really a narrow band and it would request to acquire many close images even to cover a small area.

To improve these performances, it is possible to employ a mosaic crystal, which is composed by many aligned microcrystallites acting as an aggregate. X-rays coming out have an approximately Gaussian distribution both in angle and energy. The emerging beam has an energy spread related to the crystal mosaicity and to the diffraction conditions, so the beam is monochromatic at the level of 1 keV. [19]

In addition, the shape of the beam is broader, allowing lower number of acquisitions and less time.

1.2.3 Balanced filters

The last solution provides a "virtual" monochromatization of the X-ray beam. In fact, the beams used are polychromatic and the image obtained is similar to a pseudo-monochromatic acquisition.

This is possible thanks to the use of balanced filters (Ross filters [20] [21]), which are metal foils with K-edge absorption in the interested range of the beam spectrum (in energy) and act like *low pass* filters [22]. In other words, when a Ross filter is used, the X-rays with energies above the K-edge absorption of the filter are strongly reduced, while the ones under the K-edge are less absorbed, as exemplified in Figure1.4.

Now, if we consider two filters of element Z and $Z+1$ respectively, their K-edge, at energies E_{K1} and E_{K2} , are close, so the difference in the two emerging beams will be due only to the portion between E_{K1} and E_{K2} , see Figure1.5, in this way the two filters work like a *pass band* filter [22].

The pair of filters are called Balanced filters because their thickness has to be balanced to reduce to zero in the subtraction the energies out of the two K-edges. Referring to their mass attenuation coefficient μ , the thickness of the two filters has to satisfy the following condition:

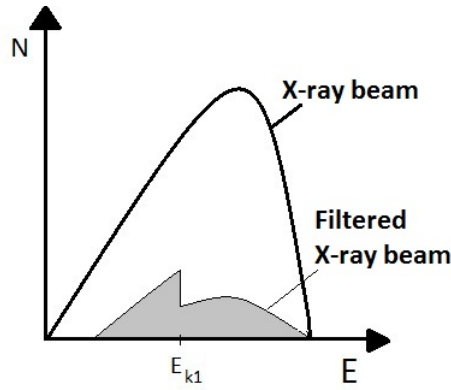
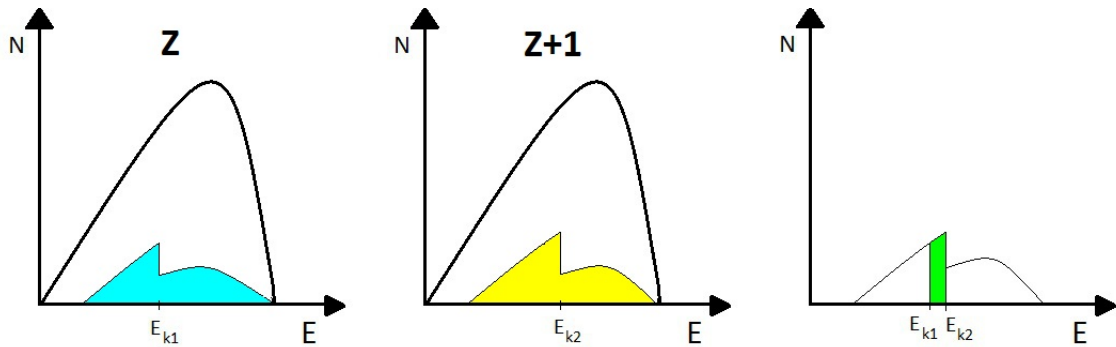


Figure 1.4: Effect of a Ross filter in a simple polychromatic X-ray beam

Figure 1.5: Difference between two beams filtered with Z and $Z+1$ elements

$$\mu_1 t_1 = \mu_2 t_2 \quad \forall E < E_{K1} \quad \text{and} \quad E > E_{K2} \quad (1.10)$$

It is important to notice that a radiography has to be acquired with each filter, then the two images are subtracted one to each other in order to obtain a new image referring to the energy range between the two K-edge absorptions. The new image is virtually acquired by a nearly monochromatic beam.

The two last methods described (1.2.2, 3.1) are portable, thanks to the use of traditional X-ray tubes and not on large facilities. The differences mainly concern the final set up. Crystals need a goniometric basis in order to select the right energies, which means more weight and occupied space. On the other hand, filters are applicable directly on the tube used for radiography, but they are less effective in monochromatizing beams.

Chapter 2

Methods and Materials

2.1 The goniometric setup

Referring to the 1st chapter, section 1.2.2, a way to monochromatize at level of 1 keV the X-ray beam produced by bremsstrahlung is by means of Bragg diffraction on a mosaic crystal. To exploit it, it is necessary to change the angle between the beam emerging from the tube and the mosaic crystal. The emerging beam will have a medium energy depending on the preset angle.

A first solution has been developed in Ferrara, where the X-ray tube and the mosaic crystal in graphite are mounted on two motorized goniometers, as reported in Figure 2.1. The X-ray source can rotate up to an angle of $2\theta = 90^\circ$, while the crystal up to $\theta = 45^\circ$, hence the quasi-monochromatic beam is always perpendicular to the sample, even if the energies employed are different.[19]

The energy range obtainable with this system is around 7-30 keV, because to obtain energies over 30 keV, the angles needed are very low ($< 4^\circ$), near to the executive limits of the set-up. However, comparing to the synchrotron, the system allows to verify also the presence of lighter Z elements as zinc or copper which have their K-edge at 9.66 keV and 8.98 keV respectively. At the first stage of this research line [19] the detection of zinc in pigment samples and paintings have been tested with good results (Figure 2.2), setting the system working at 9.0 and 10.3 keV, with the tube at 19 kV and 55 mA.

It is possible to avoid the energies of the 2nd harmonic, setting the voltage of the X-ray tube so that in the output spectrum the double energy (of the one considered) is absent, even working with light elements. In this way it is possible to eliminate in the final image the contribution of others elements (e.g. lead) which can hide the searched one.

The same device has proved to be applicable not only to lighter elements as cobalt (7.7

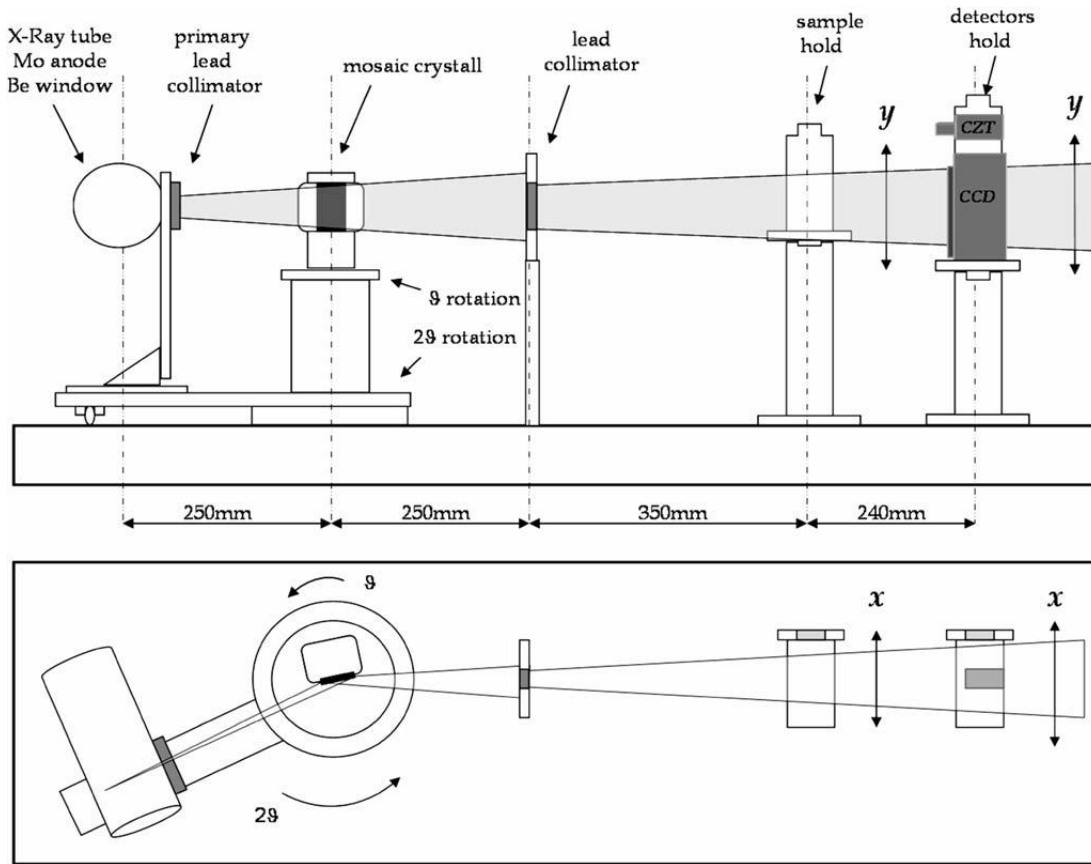
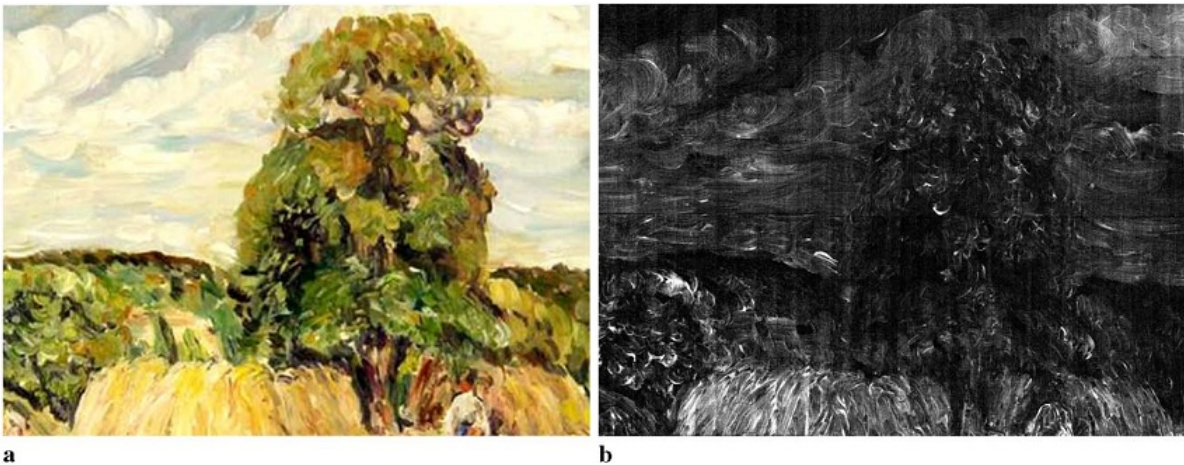


Figure 2.1: Goniometric setup from [19]

Figure 2.2: a) "La moisson a Mountfoucault", copy by Pissarro; b) Zinc thickness (ρx) distribution [19]

keV K-edge energy) and copper, but also for heavier elements as antimony (30.49 keV) and cadmium (26.71 keV). [23]

In Figure 2.3, the photo of the goniometer system used in the past [19] is reported. Starting from the right side, we have the X-ray tube which is a XM 12¹, with Molybdenum anode. The X-ray beam passes through a primary lead collimator (not visible in the photo) before impinging on the mosaic crystal, so that the dimensions of the beam are similar to those of the crystal. The mosaic crystal is a Highly Oriented Pyrolytic Graphite (HOPG)² sized 60 x 28 mm² and a mosaic spread of 0.28°. The X-ray tube and the crystal are mounted on a motorized system: two isocentric goniometers³, one for the tube and one for the crystal, are connected one over the other, in order to obtain the monochromatized beam always perpendicular to the sample and the detector. This last one is a S7199 linear CCD⁴, which has an active area of 3075 x 128 pixels of 48 μm side length.

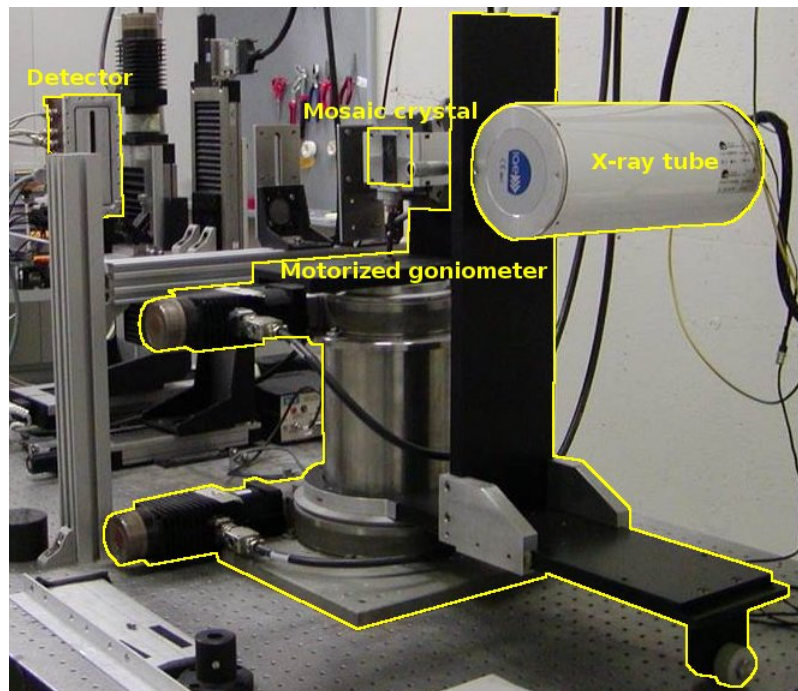


Figure 2.3: First goniometric system at the LARIX A in Ferrara

From this image and the project (Figure2.1), the overall dimensions of the device can be deduced. It is clear that this is not a portable instrument and the amount of space occupied can be easily reduced.

¹I.A.E Spa (Cormano, Italy)

²Optigraph Ltd (Berlin, Germany)

³Microcontrole (Evry, France)

⁴Hamamatsu Photonics K.K., Solid State Division (Japan)

In Figure 2.4 and Figure 2.5, the project and the photo of the new motorized goniometer are shown. As it can be seen, the main change concerns the goniometer device. The X-ray tube and the mosaic crystal are the same, while the two goniometer motors and the support on which they are mounted, have been changed. The two motors are M-060 and M-062⁵. Their accuracy in angle is of 1.2×10^{-4} and 5.5×10^{-5} respectively and the rotation range is 360° . The system has been thought to be portable, the base is easily handled.

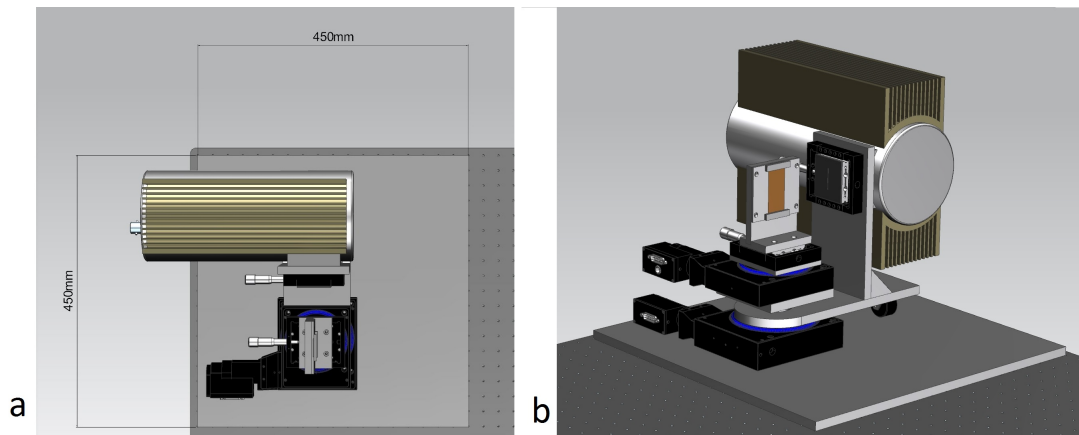


Figure 2.4: Project of the new goniometric system

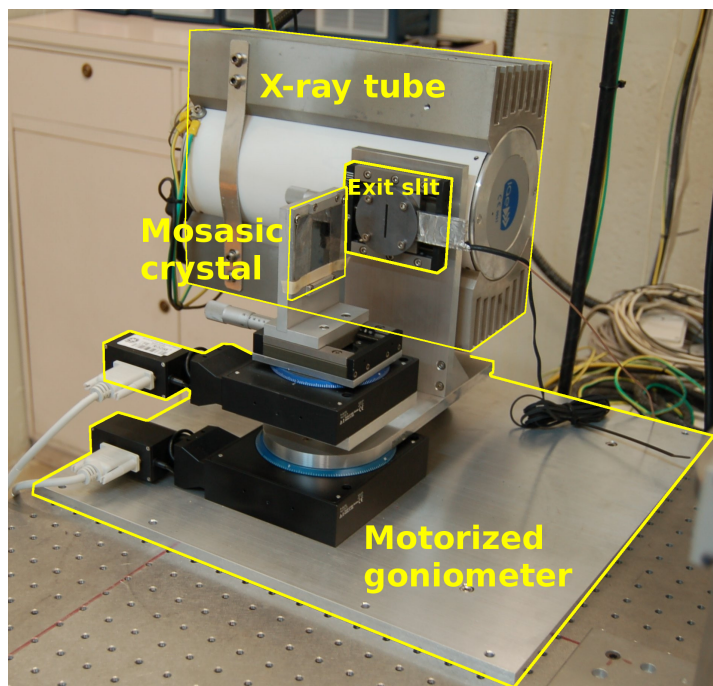


Figure 2.5: New goniometric system at the LARIX A in Ferrara

A CMOS detector was used for visualizing the emerging beam position and properly align the X-ray tube and the detector, even changing θ and 2θ . Then, a CZT detector was em-

⁵Physik Instrumente (PI) GmbH (Karlsruhe, Germany)

ployed to measure the energy spread coming out in the different positions.

The detector is the RadEye100⁶, a CMOS photodiode array with a Gd₂O₂S scintillator screen, with an active area of 98.3 x 49.2 mm², composed by 1024 x 512 pixels, 96 μm size. More in detail, the first collimator (exit slit), just out of the X-ray tube window (Figure 2.5), has to be aligned with the mosaic crystal, verifying that changing the relative angles, the position of the beam on the detector would not change.

The slit and the mosaic crystal are mounted on two micro-metric screws which have to be moved to align the system. In Figure 2.6, the images of the beam coming from the mosaic crystal at various angles (θ) are shown. The X-ray tube was set at 35 kV and 15 mA, and the time of image acquisition was 1 s. The red line in the figure indicates the center of the beam in all cases. The lighter areas on the left in c) and d), which correspond with 21.14 and 10.61 keV (calculated energies), are due to the presence of 2nd-harmonic X-rays, that will be discussed later. Anyway, they will not have any influence in the K-edge radiography, because they fall out of the definitive imaging detector.

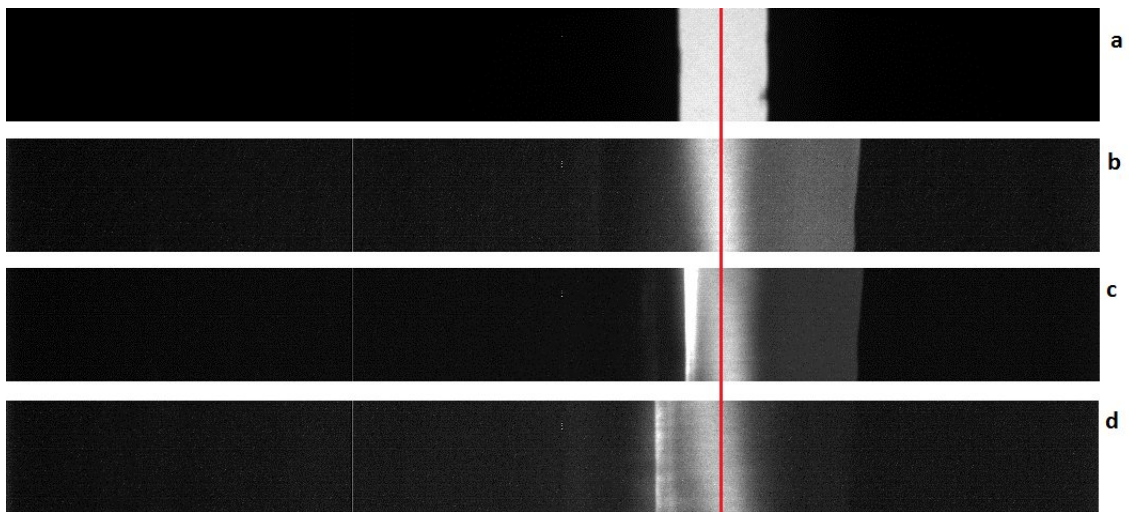


Figure 2.6: Details of the beams impinging the CMOS: a) direct beam without crystal; b) $\theta = 4^\circ$; c) $\theta = 5^\circ$; d) $\theta = 10^\circ$. X-ray tube rotated of 2θ

The Figure 2.7 is the horizontal plot of the cleanest area of the images (without the presence of 2nd-harmonic X-rays and not visible in Figure 2.6) for all the images obtained by the CMOS detector used. The grey levels are higher in the centre, which means that a larger number of photons is collected here. Furthermore, for the three different angles ($\theta = 4^\circ, 5^\circ, 10^\circ$), they are in the same position. The red line has been drawn to identify the peaks.

⁶Teledyne DALSA (Canada)

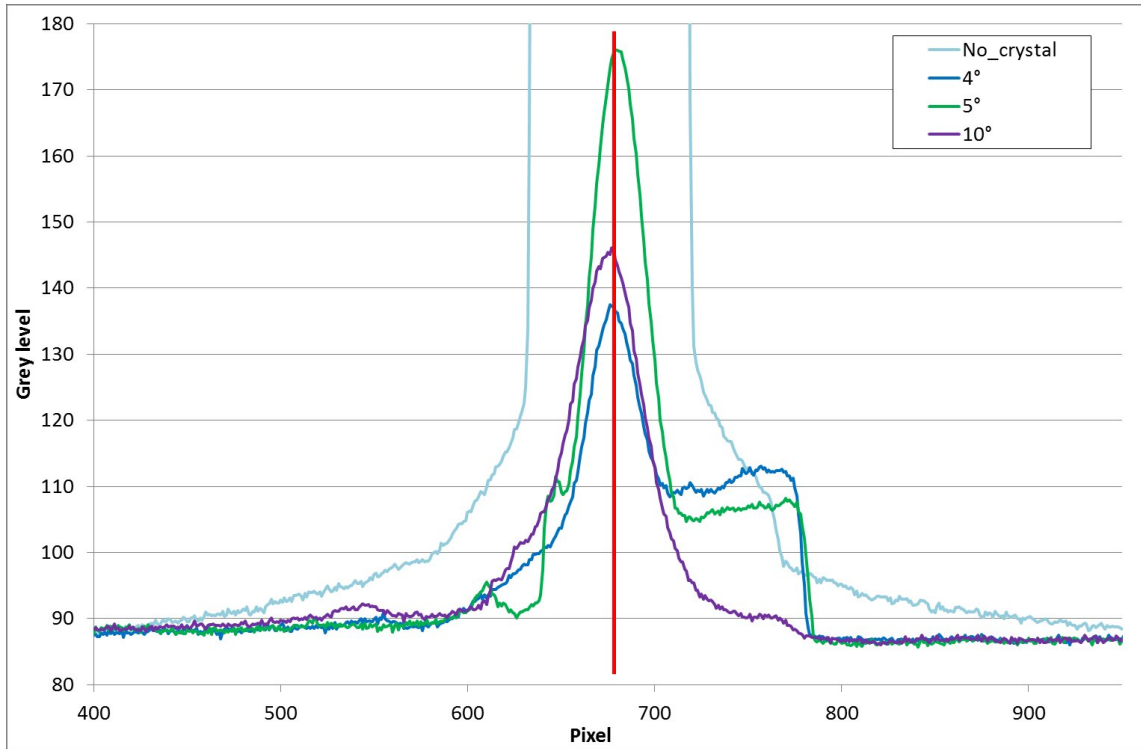


Figure 2.7: Plot of the images reported in Figure 2.6; the peak position is the same for all images

Another consideration regards the spatial distribution of the X-ray beam that arrives on the CCD detector. The XR-100T-CZT (Cadmium Zinc Telluride) detector⁷ has been used for this. It has an area of 25 mm², thickness of 2 mm, a 250 μm beryllium window and a resolution of 900 eV FWHM at 59 keV. In the range 7-40 keV, the efficiency is almost 100 %. A collimator of 224 μm diameter has been used to reduce the photon flux.

The CZT has been moved along the X axis and acquired the spectra, paying attention to the total number of photons. In Figure 2.8, the spectra at different positions (in mm) for $\theta = 7.5^\circ$ are reported. In the following graph the total counts of the peaks for each position is considered (Figure 2.9).

From the spectra, it is evident that the CZT detector is too close to the crystal and the beam arriving on it is not 1 keV bandwidth.

Furthermore, considering the dimensions of the Hamamatsu CCD detector (6.144 mm side length)(in yellow in Figure 2.9), the graph highlights that there will be a relevant difference between the number of photons impinging the centre of the detector (~ 400000 counts) and the sides (~ 250000 counts). It means that there will be a loss of sensitivity regarding the K-edge technique.

⁷Amptek (MA, USA)

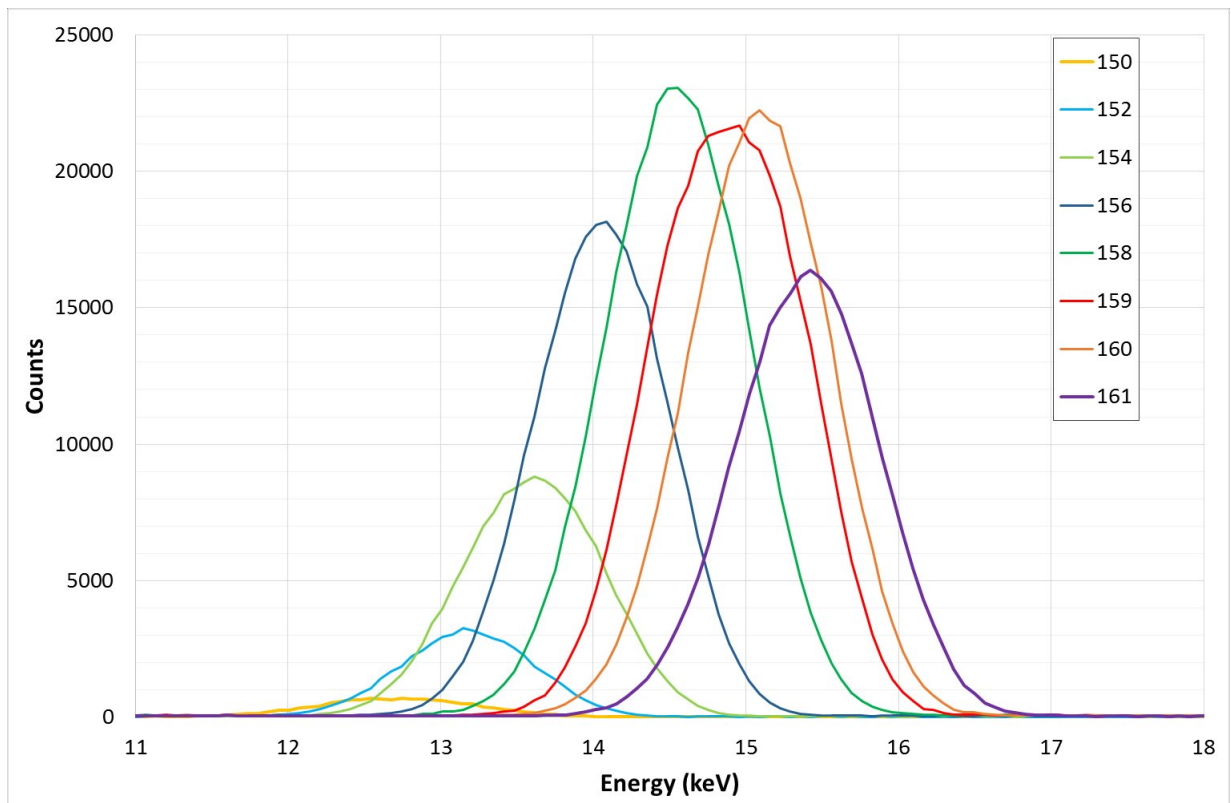


Figure 2.8: Spectra acquired at $\theta = 7.5^\circ$, changing the position (mm) of the CZT detector

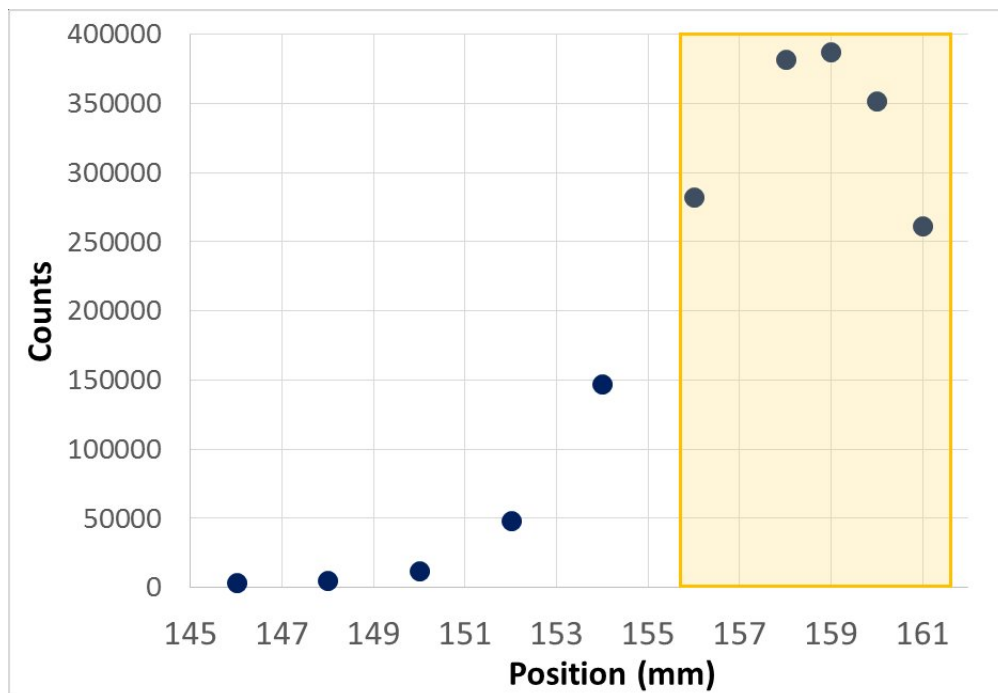


Figure 2.9: Total counts vs. CZT position of spectra reported in 2.8

At this point, it can be considered that the slit and the mosaic crystal are aligned and the direction of the beam has been identified. But the distance between the crystal and the two detectors used is not the right one, because the beam has not a narrow bandwidth (1 keV) and the number of photons is not uniform in the area covered by the CCD detector. The solution could be to distance the detectors and insert an exit collimator between the crystal and the detector.

The second step was to verify that to each angle corresponds the calculated energy. In the Table 2.1, the energies calculated for the Bragg's Law at some angles θ are listed (first two columns).

Table 2.1: Angles and energies calculated with the Bragg's Law and the measured ones

Normal		Measured	Effective	Difference
θ ($^{\circ}$)	E_c (keV)	E_r (keV)	θ_r ($^{\circ}$)	$\Delta\theta$ ($^{\circ}$)
4	26.41	28.55	3.71	0.295
5	21.14	22.46	4.71	0.295
6	17.63			
7	15.12			
7.5	14.12	14.82	7.14	0.36
8	13.24			
10	10.61	11.20	9.47	0.53
15	7.12	7.45	14.32	0.68
20	5.39			
30	3.69			

In order to verify the energies, the CZT detector has been put in the direction of the beam emerging from the crystal and acquired the spectra at various θ : 4° , 5° , 7.5° , 10° and 15° (see Figure 2.10). The X-ray tube has been set at different voltage to avoid the 2^{nd} -harmonic content in the final spectra: for 4° and 5° the voltage used was 30 kV, for 7.5° 20 kV, for 10° 19 kV, and for 15° 10 kV.

From the spectra, measuring the energies of the peaks (3^{rd} column in Table 2.1), it has been found that there is a slight difference between the obtained energies and the calculated ones (2^{nd} column). Furthermore, it was evident from the spectra that at small angles (4°), there is the direct contribution of the non-diffracted X-rays coming from the source (at 17.48 keV there are the K_{α} lines of molybdenum).

Starting from these measured energies, the angles of diffraction have been calculated (4^{th} column in Table 2.1) to obtain a corrective factor for θ and 2θ of the cases analysed (5^{th} column). For example, considering $\theta = 4^{\circ}$, the energy measured by the spectrum is 28.55 keV, instead of 26.41 keV. This means that the real angle is smaller than the one setted, and it is of 3.7° . So, if we want to obtain 26.41 keV we have to sum 0.3° to

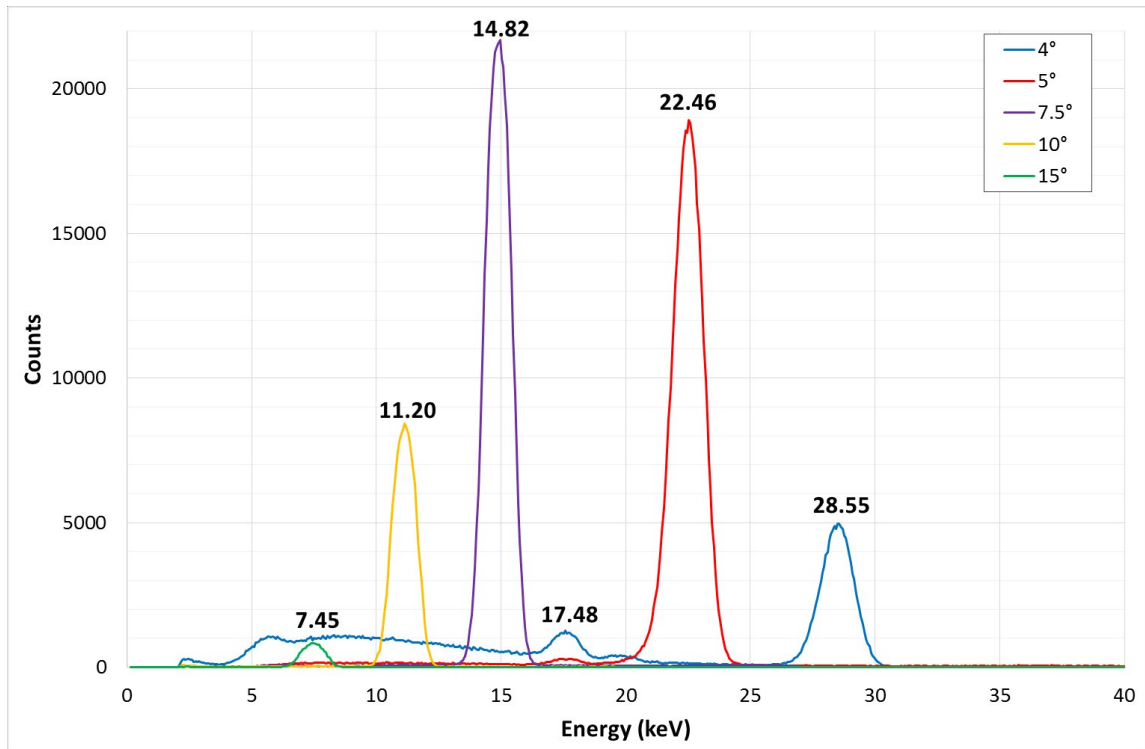


Figure 2.10: CZT spectra acquired at different angles

the calculated angle. In Figure 2.11 the spectra acquired at nominal 4° and 4.3° are shown.

Unfortunately, the corrective factor is not the same for other angles, even if the Figure 2.7 seems to indicate that the alignment is correct for each angle, probably because the resolution of the CMOS detector is low. An hypothesis can be that not the perpendicular beam to the tube, but an oriented one has been selected, impinging on the crystal with a specific angle. This angle is different for each θ and 2θ . Further tests are necessary to correct this misalignment.

Then, referring to image *d* in Figure 2.6, the nature of the band on the left of the main beam has been investigated. Fixing θ to 10° , which corresponds to a measured energy of 11.20 keV, the CZT has been moved in the image plane, along the horizontal axis by step of 2 mm, starting from the orthogonal position, to find the energies involved. Some of the measured spectra are reported in Figure 2.12.

The X-ray tube was set at 30 kV, the same condition of the acquired images. In the spectra the X-rays of the 2^{nd} order at energies around 20 keV are evident. At 8 mm of displacement, while the peak around 10 keV decreases, the peak of the X-rays of the 2^{nd} harmonic reaches the same number of counts. This is due to the K_β line of fluorescence of the Molybdenum. In other words, in this condition, the angular spread of the mosaic crystal and the voltage applied to the tube allow the fluorescence line at 19.9 keV of the

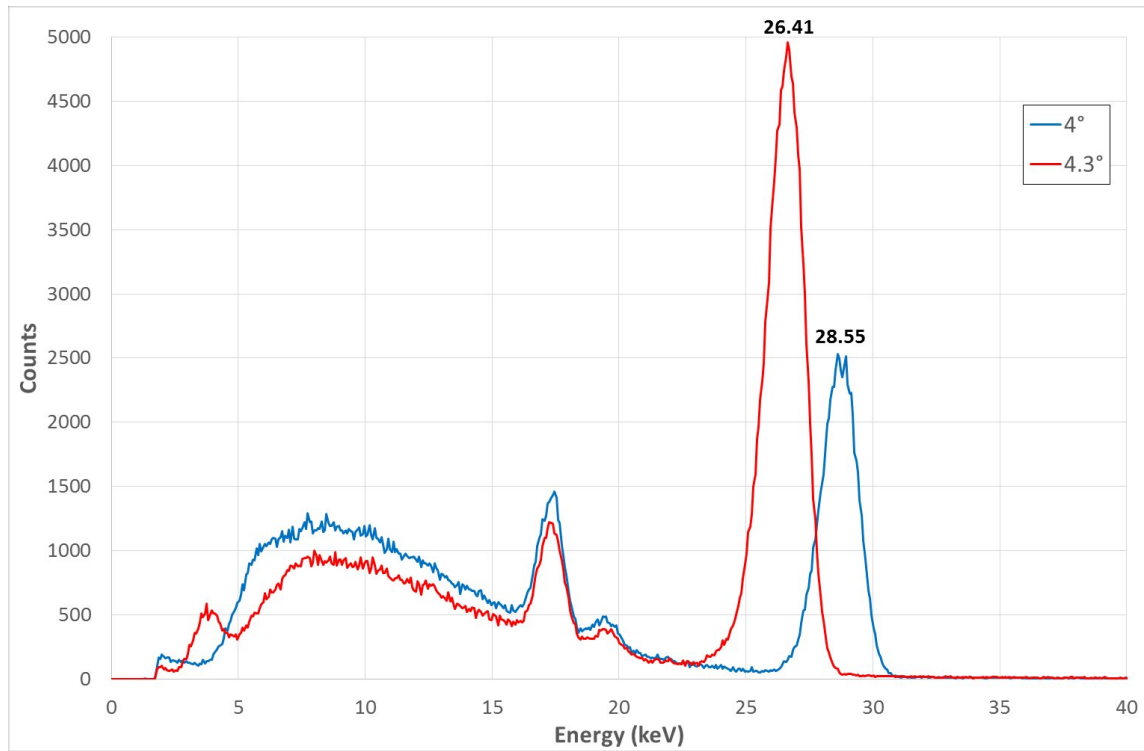
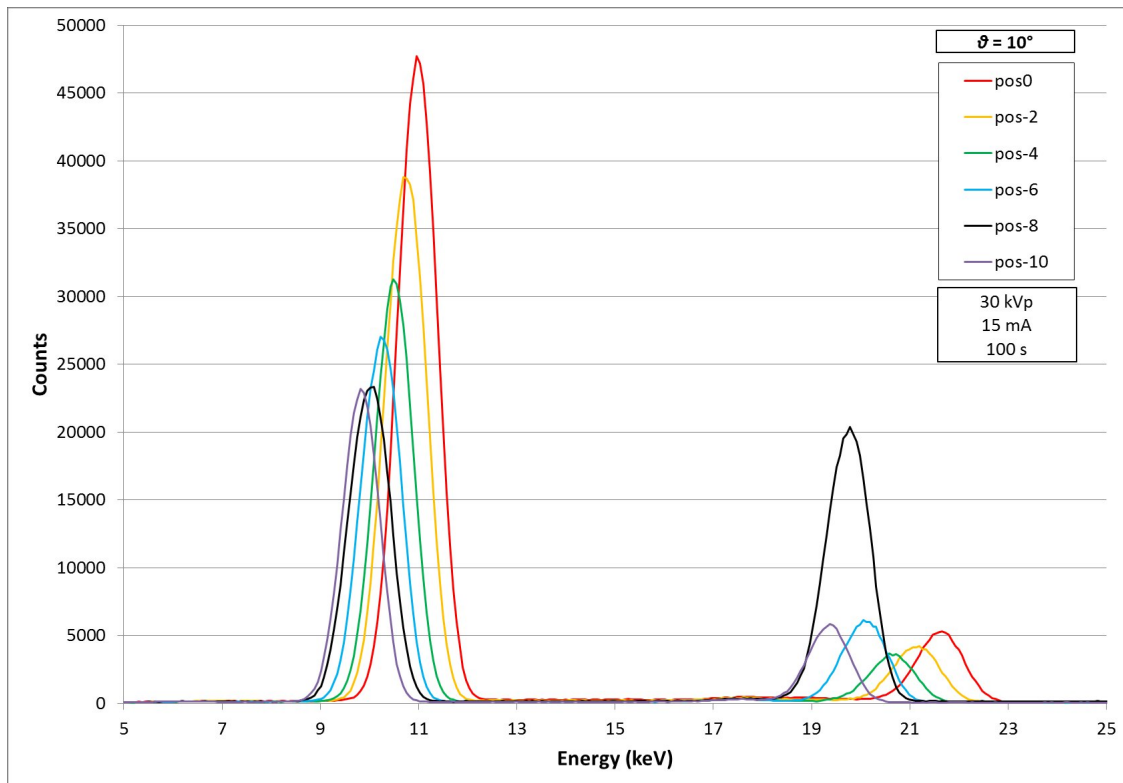
Figure 2.11: CZT spectra at 4° and 4.3° 

Figure 2.12: CZT spectra acquired in different positions

anode to be diffracted.

Even if the contribution of others energies decreases the contrast in the K-edge radiography, it should be considered that the harmonic energies can be avoided, choosing the best settings of the source. Furthermore, the line is at 8 mm from the centre of the main beam, and the Hamamatsu CCD has an active area large 6 mm, so the molybdenum lines will not be acquired.

2.2 The balanced filters

In the last years some tests have been performed using balanced filters for detecting cadmium [24]. Cadmium has a K-edge energy of 26.7 keV and the balanced filters used and their thickness are listed in Table 2.2.

Table 2.2: Balanced filters for Cadmium

Element	Energy (keV)	Thickness (μm)
Ag	25.5	102
Cd	26.7	129
In	27.9	147

The molybdenum anode X-ray tube, a Varian M-143T, with 39 kV_{max}, has been used for working on cadmium, while the previous work used the tungsten anode [24]. In the image below (Figure 2.13), the spectra of the filtered beam for Cd are shown. The source was set at 35 kV and the acquisition lasted 5 min.

Also copper and cobalt has been investigated with the balanced filters. These two elements are very common in pigments, but their K-edge have lower energies than cadmium, so mapping their presence could be tricky.

The energies involved and the relative filters used are listed in the following table (Table 2.3).

It has been calculated that the thickness for the copper foil should be 9.22 μm , for Nickel 9.84 μm and for Zinc 10.4 μm , but the commercial size of 10 μm thick has been chosen for the three. The calculated transmission of these filters is reported in Figure 2.14.

The spectra transmitted by each filter, working at 20 kV, 19 mA and acquiring for 1 s, are reported in Figure 2.15. The X-ray tube worked at low voltage to avoid the presence of molybdenum fluorescence lines. Furthermore, the filters have been doubled in order

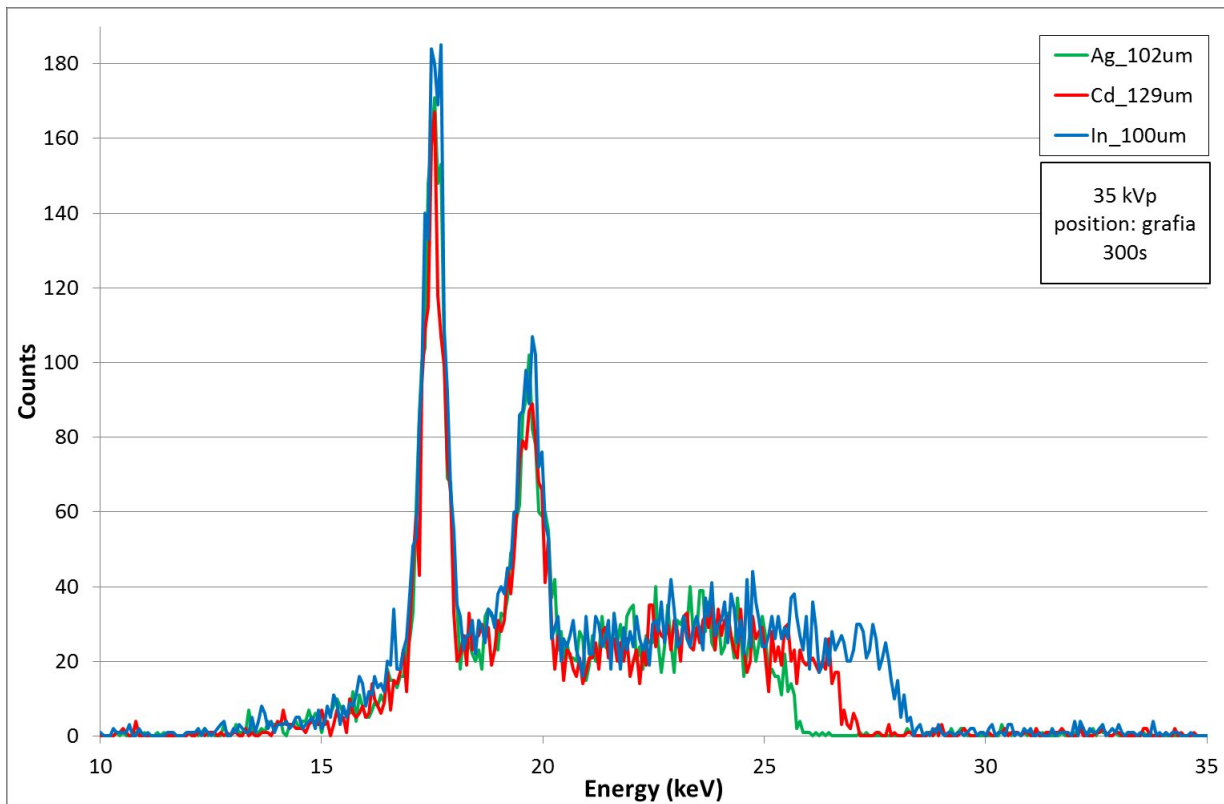


Figure 2.13: CZT spectra of the X-ray beam filtered by 3 filters used with the Mo source. The peaks at 17.4 and 19.9 keV are the fluorescence lines of the anode

Table 2.3: Balanced filters for Cobalt and Copper

Element	Energy (keV)	Thickness (μm)
Fe	7.1	10
Co	7.7	7
Ni	8.3	10
Element	Energy (keV)	Thickness (μm)
Ni	8.3	10
Cu	9.0	10
Zn	9.7	10

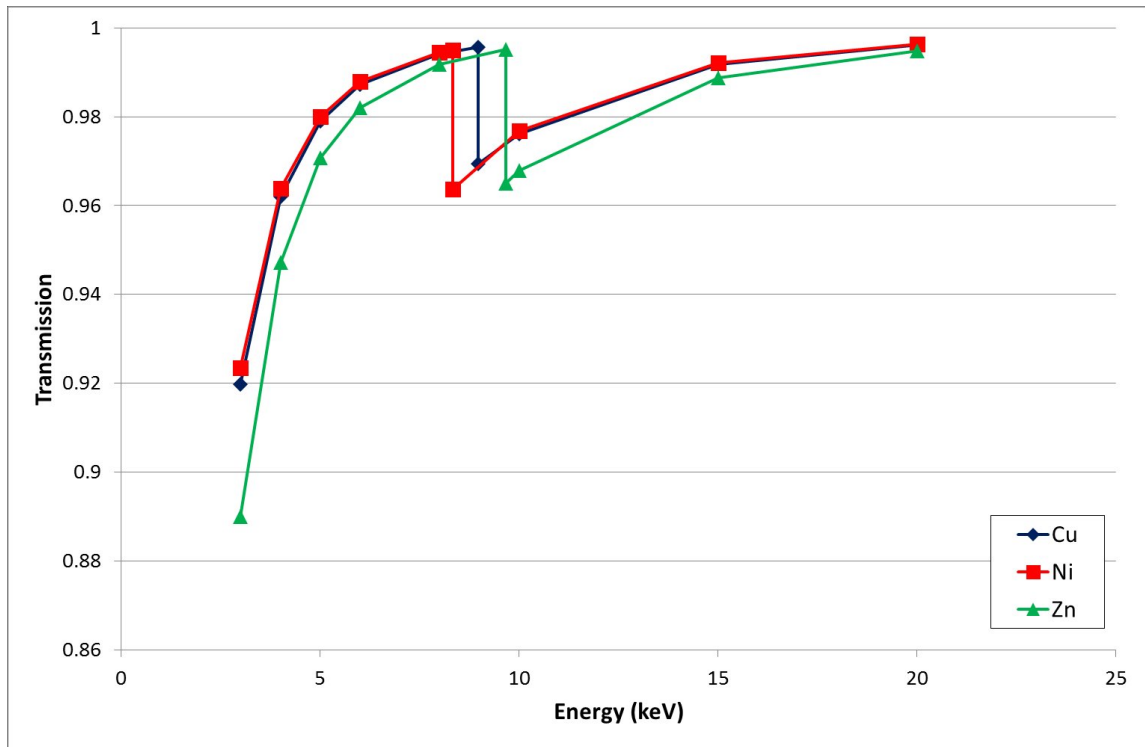


Figure 2.14: Calculated transmission of Cu, Ni and Zn filters 10 μm thick

to obtain the better compromise between the X-rays transmitted at low energies (the K-edges area) and at high energies. These last could decrease the contrast in the final image.

It is important to note that the subtraction of these spectra carries out virtual beams of 0.7 keV bandwidth, narrower than cadmium ones.

Coming to the Cobalt, the thickness calculated for each filter should be:

- for Fe, 9.97 μm
- for Co, 7.36 μm
- for Ni, 10.4 μm

The commercial thicknesses of the filters used are reported in Table 2.3. In this case, due to the very low energies employed, the thickness of filters has not be doubled, because the absorption of X-rays in that region strongly depends on the thickness crossed.

The CZT spectra (Figure 2.16), obtained at the same condition of copper, show that the bandwidth of the virtual beams are even narrower than the previous cases (0.6 keV). Considering the shape of Fe and Co spectra, it can be deduced that in the K-edge area the thickness has a relevant effect in the absorption of X-rays. In fact, it can be noted that the Nickel spectrum has a clear cut at around 8 keV, while the other two have a

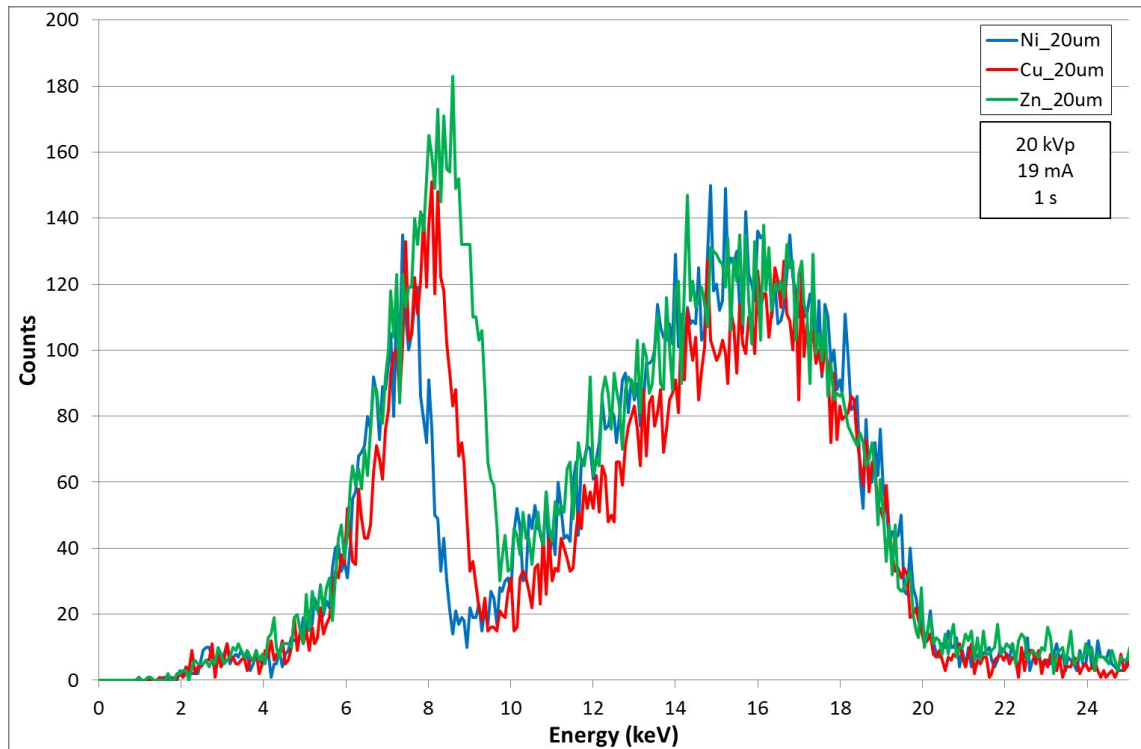


Figure 2.15: CZT spectra of the filters for the identification of Copper

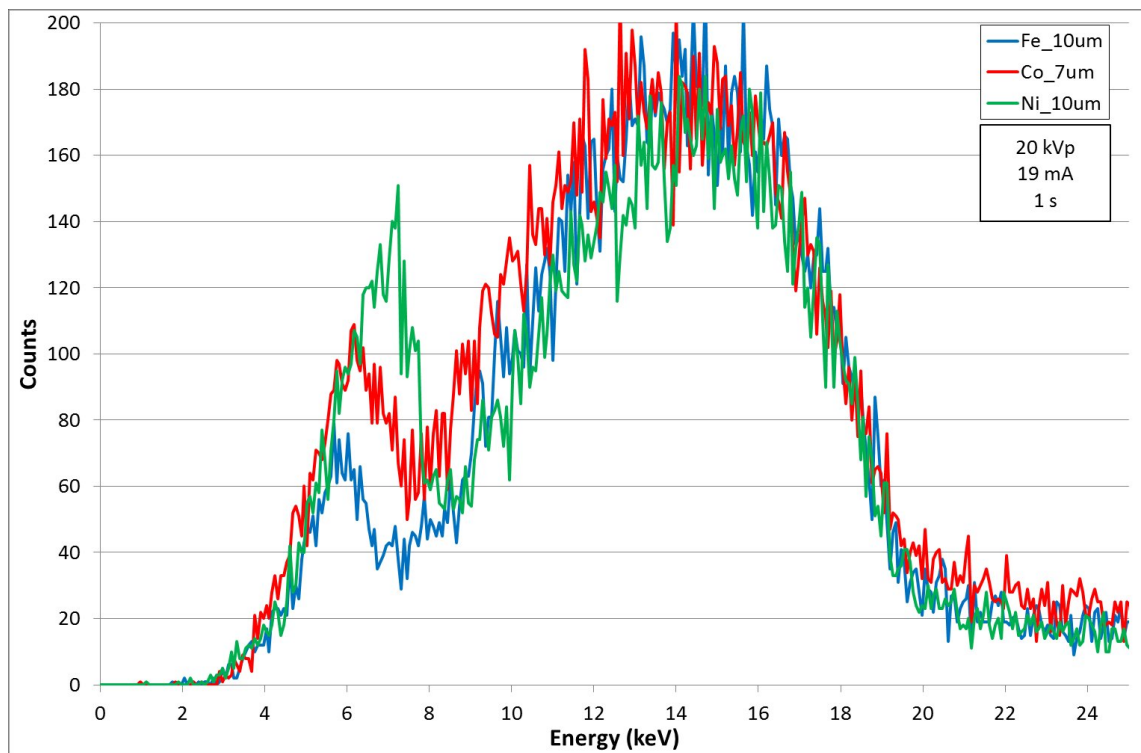


Figure 2.16: CZT spectra of Iron, Cobalt and Nickel filters

broader trend, that could influence the contrast in the K-edge radiography of Cobalt.

In addition, it should be considered that the imaging detector can be less efficient at around 7-8 keV, so it is evident that revealing cobalt could be even more difficult than cadmium and copper.

2.3 The radiographic scanner

As well known, the digital radiography arises many advantages compared with the traditional radiography:

- the visualization of the radiographic image is immediate,
- the range of grey level is bigger (4096 for 12-bit digitization vs. 100 of old X-ray plates),
- the digital elaboration implies no segmentation and best uniformity in the final radiography of the whole painting.

Scanning systems allow to exploit all these advantages and, furthermore, due to the motorized movement of the source and the detector, the time employed to scan whole paintings is reduced. At the Dept. of Physics and Earth Science of Ferrara, collaborating with INFN, two scanning systems for radiography have been developed: the first allows to analyse big paintings and the alignment between the source and the detector is always verified, the second is a more portable device for *in situ* radiography.

In Figure 2.17, the first scanner for radiographies developed by the University of Ferrara, INFN of Ferrara and TekneHub, is illustrated. It has been designed to perform the radiography of large paintings up to 1.5 x 2.5 m. The X-ray tube (Varian M-147 with anode of Molybdenum) and the Silicon detector (Teledyne DALSA RadEye200, a CMOS photodiode array with Gd₂O₂S scintillator screen, 1024 x 1000 pixel, 96 μ m side length and 12 bit/pixel of digitization) are mechanically bounded to ensure the alignment between them. They move together thanks to motorized guides, for the two axis. [25] [26] Due to its dimensions (2.56 x 2.26 x 1 m), the transport of the scanner is not easy and cannot be considered easily transportable.

Starting from this instrument, a new scanner for *in situ* radiography has been developed by the University of Ferrara in collaboration with INFN. The main task was to have a really transportable RX scanner, easier to be transported and assembled. [27]

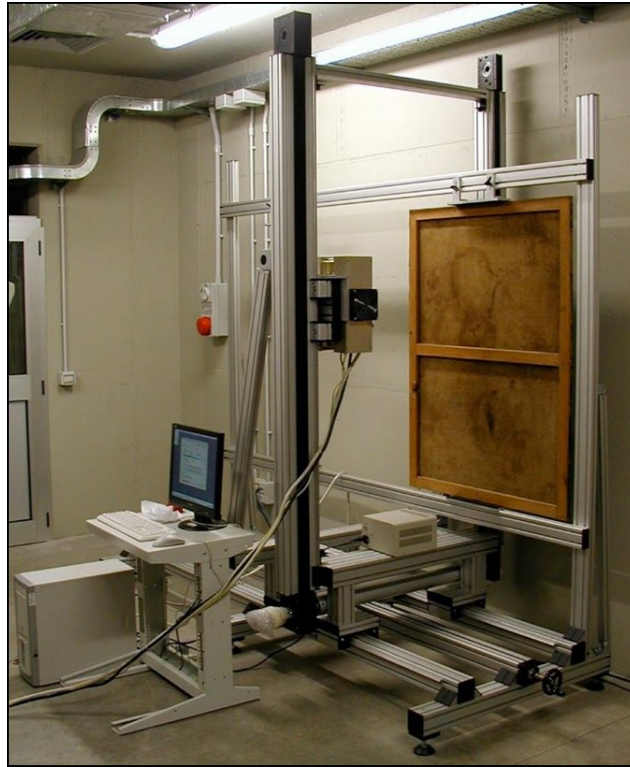


Figure 2.17: First transportable scanner for *in situ* radiography



Figure 2.18: The new radiographic scanner at the Regional Gallery of Palazzo Bellomo, Siracuse

The new RX scanner is composed by two units, one for the X-ray tube and one for the detector, and they are not bounded together (Figure 2.18). The dimensions of each unit are 1.40 x 1.53 x 0.74 m and their weight is ~ 55 kg. The system allows to scan an area of 1 m², but as there is no mechanical bound between the two stages, there is no limitation in the size of the painting to analyse.

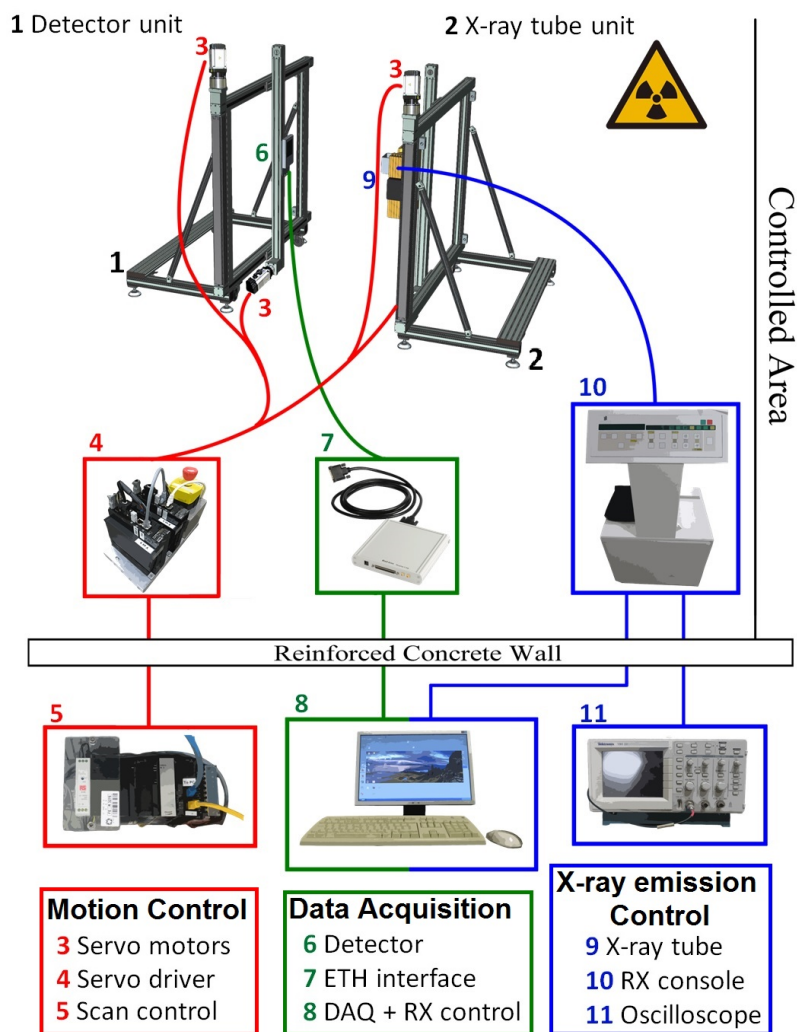


Figure 2.19: Devices connection diagram of the new RX scanner [27]: the Motion Control (red), the Data Acquisition (green) and the X-ray emission Control (blue)

In Figure 2.19, the connection among all the devices is summarized. Each unit is equipped with two AC servo motors (G5⁸) for the motion along X and Y axis of the X-ray tube and the detector, they are connected to the servo drivers directly on the stage and, through it, to the control system via Ethernet. The scan control system commands:

- the motion speed: from 5 up to 50 mm/s

⁸Omron Electronics Ltd, UK

- the scanning mode: performed in horizontal as coil or straight lines mode
- the number of steps (in X and Y) and the distance between two consecutive positions.

Furthermore, there is a 1 m linear rail (KLE60⁹) for each axis, with accuracy of repeatability given at 0.02 mm. So the positions can be precisely reached again.

The RadEye200 detector is connected via Ethernet to the DAQ station, where the ShadoCam software¹⁰ operates the acquisition of the images. The same station controls also the X-ray shots, according to the parameters set on the RX control. The X-ray tube is a Varian M-143t, 49 kV_{max}, 500 mAs_{max} and air cooled. The control of the X-ray emission is performed by the oscilloscope located near the control station.

Before starting the acquisition of the radiographic images, the two units must be levelled and aligned. The first is performed by setting the levelling feet, then a first alignment is carried out using mechanical plugs that fasten the units. The precise alignment is made using a small pinhole in front of the X-ray tube. The beam coming out should centre a target pixel of the detector; if not, the tube or the detector can be moved. In this way, the alignment can be immediately verified during the acquisition without taking off the painting.

A long time has been dedicated to the alignment of the two units. At the beginning, indeed, the misalignment along the X and Y axis in a scanned line was of 8 mm. The first operation was to change the ratio between the support movement and the motors rotation, in order to reduce the misalignment to 1 mm for X and 4 mm for Y. Then, in order to maintain the two units parallel among them, the problem about the levelling has been resolved thanks to the mechanical bound carried out by the plugs. Following the procedure described before, the misalignment along a scanned line has been reduced to few tenths of millimetre in X and 1.5 mm in Y.

The acquisition of the images occurs when the X-ray tube and the detector are stationary. Usually there is at least 20% of overlapping between two consecutive radiographies. The stitching of images is automatically performed by the PTGui 10[©] software¹¹, after their correction.

Several tests have been performed in order to align, calibrate and tune the system. All these tests allowed to identify the best procedure to be followed. Finally, the new radio-

⁹ITEM Industrietechnik GmbH (Germany)

¹⁰Rad-Icon Imaging Corp (Santa Clara, CA, USA)

¹¹New House Internet Services BV, the Netherlands

graphic scanner has been applied also *in situ*. For the 3rd Training Camp of IPERION-CH.it (25-30 September 2016), promoted by INFN and CNR, it has been moved from Ferrara to Siracusa, at the Regional Gallery of Palazzo Bellomo, for one week. The radiographies performed have highlighted potentialities and disadvantages of this device.



Figure 2.20: Photo of the new RX scanner at Palazzo Bellomo during the acquisition of the RX of the *Virgin Mary in throne with the Child*

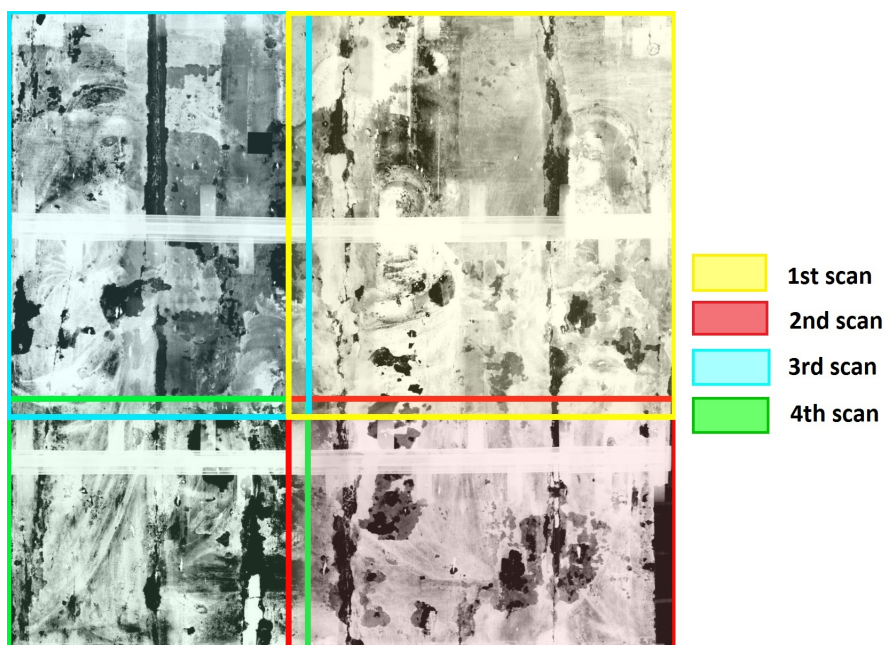


Figure 2.21: Acquisition scheme for the radiography of *Virgin Mary in throne with the Child*

The analysed works were paintings on wood of the XV century. One of them was a "Virgin Mary in throne with the Child" (Figure 2.22) of big size: 195 x 154 cm. This case has shown the adaptability of the RX scanner to paintings of various dimensions. In Figure

2.20, the scan of a part of the painting is shown.

Due to its dimensions, the radiography of the whole painting was possible in four steps. The painting has been divided in quarters (Figure 2.21): the first took 196 images and 1 h 45 min time of acquisition, the second 126 images and 1 h 30 min, the third 140 images and 1 h 25 min, and the last 100 images in 1 h.

Then, the total scanned area was covered by 562 radiographic images (considering that some lines are overlapping for the final stitching) and required 5 h and 40 min. The final radiography is reported in Figure 2.23.



Figure 2.22: Anonymous, *Virgin Mary in throne with the Child*, wood, 195 x 154 cm, Siracuse, Palazzo Bellomo Museum. This work of art is composed by 4 superposed paintings with the same theme of different historic period.



Figure 2.23: Radiography of *Virgin Mary in throne with the Child*, composed by 562 images acquired with the X-ray source at 26 kV and 19 mA, filtered with 0.18 mm of Aluminium and acquisition time of 2 s. The aim of the radiography was to identify and virtually separate the four layers.